PLEATED FILTER DESIGN BY COMPUTER SIMULATIONS

A. WIEGMANN, L. CHENG, E. GLATT, O. ILIEV AND S. RIEF
FRAUNHOFER ITWM, KAISERSLAUTERN, GERMANY

Abstract. Four aspects are important in the design of hydraulic filters. We distinguish between two cost factors and two performance factors. Regarding performance, filter efficiency and filter capacity are of interest. Regarding cost, there are production considerations such as spatial restrictions, material cost and the cost of manufacturing the filter. The second type of cost is the operation cost, namely the pressure drop. Albeit simulations should and will ultimately deal with all 4 aspects, for the moment our work is focused on cost.

The PleatGeo Module generates three-dimensional computer models of a single pleat of a hydraulic filter interactively. PleatDict computes the pressure drop that will result for the particular design by direct numerical simulation. The evaluation of a new pleat design takes only a few hours on a standard PC compared to days or weeks used for manufacturing and testing a new prototype of a hydraulic filter. The design parameters are the shape of the pleat, the permeabilities of one or several layers of filter media and the geometry of a supporting netting structure that is used to keep the outflow area open. Besides the underlying structure generation and CFD technology, we present some trends regarding the dependence of pressure drop on design parameters that can serve as guide lines for the design of hydraulic filters. Compared to earlier two-dimensional models, the three-dimensional models can include a support structure.

Keywords: Solid-Gas Separation, Solid-Liquid Separation, Pleated Filter, Design, Simulation.

1. Introduction

Pleated filter panels are used in a variety of industrial applications, both for gas and liquid filtration. A pleated filter has a reduced pressure drop and improved particle collection efficiency compared to a flat sheet at the same base area [1]. For a given filter media and pleat height, for a low pleat count the pressure drop increases due to the reduced surface area of the filter media. For a high pleat count, the pressure drop increases due to viscous drag in the channels. Thus, there exists an optimal pleat count that has the lowest pressure drop for given filter media and pleat height [1]. Similar effects exist also when a support structure is used to keep the outflow and inflow channels of the pleat open. This structure, yet it obstructs the channel and the surface of the support structure effectively, also reduces the available surface area of the filter media.

Designing pleats by numerical simulations has been the objective of several studies in the past. In the absence of a support structure, two-dimensional simulations suffice [1, 8, 7, 9]. Truly three-dimensional pleat property simulations are now becoming feasible due to better models and increased computer power [11]. Several ways of coupling the free flow in the channels with the porous media flow in the media were tried: From Darcy-Lapwood-Brinkmann [1], Stokes-Darcy [8, 7, 9] to Stokes-Brinkmann [5, 11]. Also, on the discretization side, different methods were tried: from finite elements [1, 8, 7, 9] to finite volumes on collocated grids [5], a Lattice-Boltzmann approach in [11] and finally here we use the SIMPLE method [6] on staggered grids [4]. In all the literature, a single pleat is looked at to decrease the required computational power. It is sometimes referred to as the repetitive unit or periodicity cell.

In this work, a simple to use integrated simulation tool for the design of pleated filter panels is described and validated. The tool

- creates the pleat from parameters such as pleat height, pleat count, media thickness etc.
- creates nettings and woven support structures adapted from [3].
- allows to assign the permeability to one or several layers of the filter media.
- automatically sets up the computational grid and boundary conditions.
- computes the pressure drop from flow rate, fluid density and fluid viscosity [2].

Date: April 27, 2009.
e-mail: (wiegmann, cheng, glatt, iliev, rief)@itwm.fraunhofer.de.

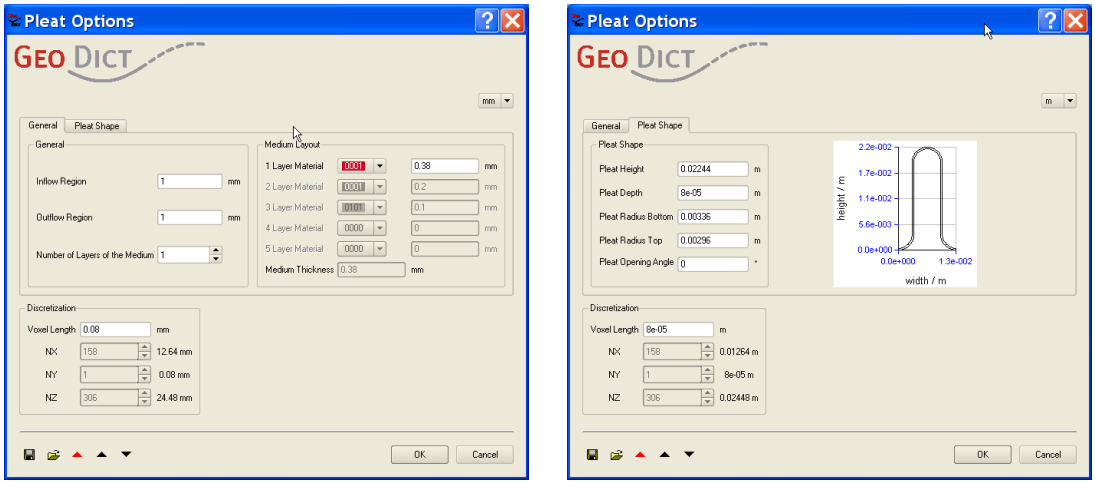

a) b)

FIGURE 1. *a) General pleat options and b) Pleat shape options. Setting the pleat depth to the voxel length conveniently creates the two-dimensional computational grid.*

2. VIRTUAL PLEATS

A virtual pleat is generated completely automatically from a few parameters. For the simplest case without support structure, the parameters are

- Inlet length (inflow region)
- Outlet length (outflow region)
- Up to 5 layers and thickness for each
- Pleat depth (a single voxel for 2d simulations)
- Pleat height
- Layer material types
- Pleat opening angle
- Pleat radius at inlet (pleat radius top)
- Pleat radius at outlet (pleat radius bottom)
- Voxel length (the resolution for the simulation)

Figure 1 illustrates how the parameters are entered into the graphical user interface (GUI). Changing the height, radii (i.e. the pleat width) or opening angle are instantaneously illustrated by a drawing.

For pleated structures with supporting netting or supporting mesh, the depth of the pleat is chosen automatically as a repetitive cell of the netting or the woven structure. Additional parameters in this case are two wire diameters, the pitch in both directions (the aperture is then automatically determined from wire thickness and pitch), the wire overlap, the impression depth of the wires into the media, the type of weave etc. Figure 2 a) - c) illustrate how the additional parameters get entered into the GUI.

Figure 2 d) illustrates how the data is used for a parameter study in the case of a pleat without a supporting structure. In the first block of the .gvm (for GeoDict vary macro) file, the parameters for the pleat structure generation are specified. In this case, variables for the pleat height (% 2) and the pleat width (% 3, % 4) are used, because these are parameters varied in an example from the literature [1] that is reproduced in the results section. In the second block of the .gvm file, the parameters for the computation of the pressure drop are specified. Again, a variable (% 1) is used to vary the permeability of the media. Three more variables are used to create a meaningful file name for the parameter study, namely the media identity number (% 5), the pleat height (% 6) and the pleat count (% 7). The values for all variables are defined in the calling .gmc (for GeoDict macro) file, see Figure 3.

The media is determined by its name (Variable 5 or %5 in the .gvm file), which is chosen as in [1], and by its permeability (Variable 1 or % 1 in the .gvm file). The height is given in [mm] as used in GeoDict (Variable 2 or % 2 in the .gvm file) and in [inch] as it was used in [1] (Variable 6 or % 6 in the .gvm file). Finally, the width is defined by the pleat count (pleats per inch) as in [1] (Variable 7 or % 7 in the .gvm file), which defines the bottom and the top radius, i.e. radius near the outlet and inlet of the pleat, used in GeoDict

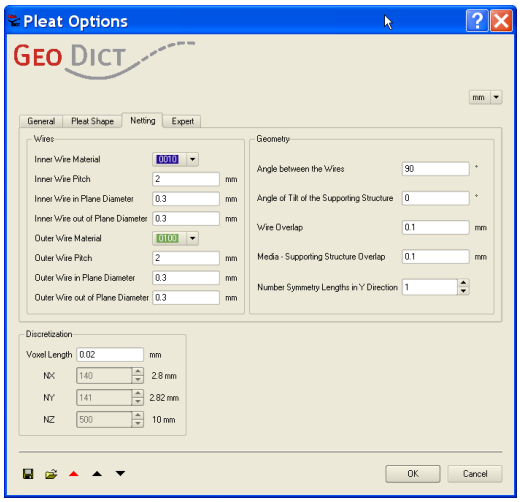

a)

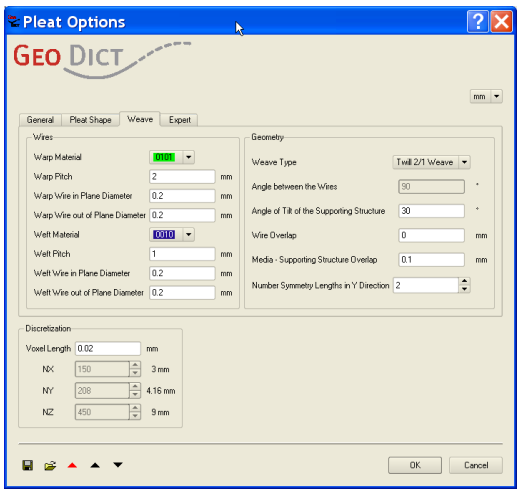

b)

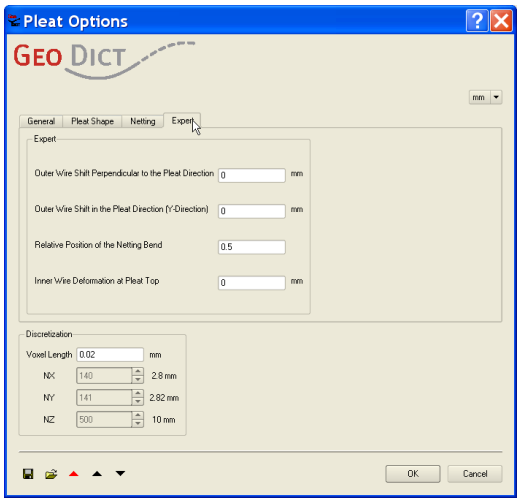

c)

```
PleatGeo:WithoutSupportingMesh {
FileName
InflowRegion 0.001
MediaThickness1 0.0004
MediaThickness2 0
MediaThickness3 0
MediaThickness4 0
MediaThickness5 0
NumberLayers 1
OutflowRegion 0.001
PleatDepth 8e-05
PleatHeight %2
PleatMaterial1 1
PleatMaterial2 0
PleatMaterial3 0
PleatMaterial4 0
PleatMaterial5 0
PleatOpeningAngle 0
PleatRadius1 %3
PleatRadius2 %4
VoxelLength 8e-05
}

PleatDict:SolveEFVStokesBrinkmann {
NumberOfNodes 1
Parameters:FluidDensity 1.204
Parameters:FluidViscosity 1.834e-05
Parameters:MeanVelocity 0.508
Parameters:PressureDifference 0.02
Parameters:PressureEnabled 0
Permeabilities:Color1 %1,%1,%1
Permeabilities:Color10 0,0,0
Permeabilities:Color11 0,0,0
Permeabilities:Color12 0,0,0
Permeabilities:Color13 0,0,0
Permeabilities:Color14 0,0,0
Permeabilities:Color15 0,0,0
Permeabilities:Color2 0,0,0
Permeabilities:Color3 0,0,0
Permeabilities:Color4 0,0,0
Permeabilities:Color5 0,0,0
Permeabilities:Color6 0,0,0
Permeabilities:Color7 0,0,0
Permeabilities:Color8 0,0,0
Permeabilities:Color9 0,0,0
RelaxationPressure 0.8
RelaxationVelocity 0.5
SolverData:Accuracy 1e-05
SolverData:AddedFreeSpace 0
SolverData:DirectionEnabledX 0
SolverData:DirectionEnabledY 0
SolverData:DirectionEnabledZ 1
SolverData:DiscardTemporaryFiles 0
SolverData:FileName Pleat_%5_%6_%7.gdr
SolverData:MaxNumberOfIterations 100000
SolverData:MirrorVolume 0
SolverData:NumberOfProcesses 8
SolverData:PermeabilityCheckInterval 20
SolverData:Restart 0
SolverData:RestartFileName
SolverData:ScalingType 1
SolverData:ScalingValue 1
SolverData:SlipLength 0
SolverData:SolverType 0
SolverData:StoppingCriterion 1
}
```

d)

FIGURE 2. *a) Netting support pleat options and b) Weave support pleat options. c) Expert pleat options and d) GeoDict Vary Macro File. The .gvm file contains the two commands that perform a parameter study namely the generation of the pleat and the computation of the pressure drop. The variables %1-%7 indicate the quantities that are varied under the parameter study.*

```
GeoDict:VaryMacro{
  FileName pui.gvm
  NumberOfVariables 7
  Variable1:ValueList 7.25e-13,1.03e-12,2.26e-12,3.20e-12,7.68e-12,1.10e-11
  Variable1:CoupledWith NONE
  Variable2:ValueList 0.02224,0.04448,0.08888,0.13336
  Variable2:CoupledWith NONE
  Variable3:ValueList 0.00336,0.00232,0.00176,0.00144,0.00128,0.00112,0.00096,0.00088,0.00080,0.00072,0.00064,0.00056,0.00056,0.00048
  Variable3:CoupledWith NONE
  Variable4:ValueList 0.00296,0.00192,0.00136,0.00112,0.00088,0.00072,0.00064,0.00048,0.00048,0.00032,0.00024,0.00024,0.00016,0.00016
  Variable4:CoupledWith 3
  Variable5:ValueList 252,213,233,220,224,229
  Variable5:CoupledWith 1
  Variable6:ValueList 0.875in,1.750in,3.500in,5.250in
  Variable6:CoupledWith 2
  Variable7:ValueList  2, 3, 4, 5, 6, 7, 8, 9,10,12,14,16,18,20
  Variable7:CoupledWith 3
}
```

FIGURE 3. *The GeoDict Macro File defines the values for the parameter study and calls the commands that perform the study in the .gvm file [Figure 2 d)] with these values.*

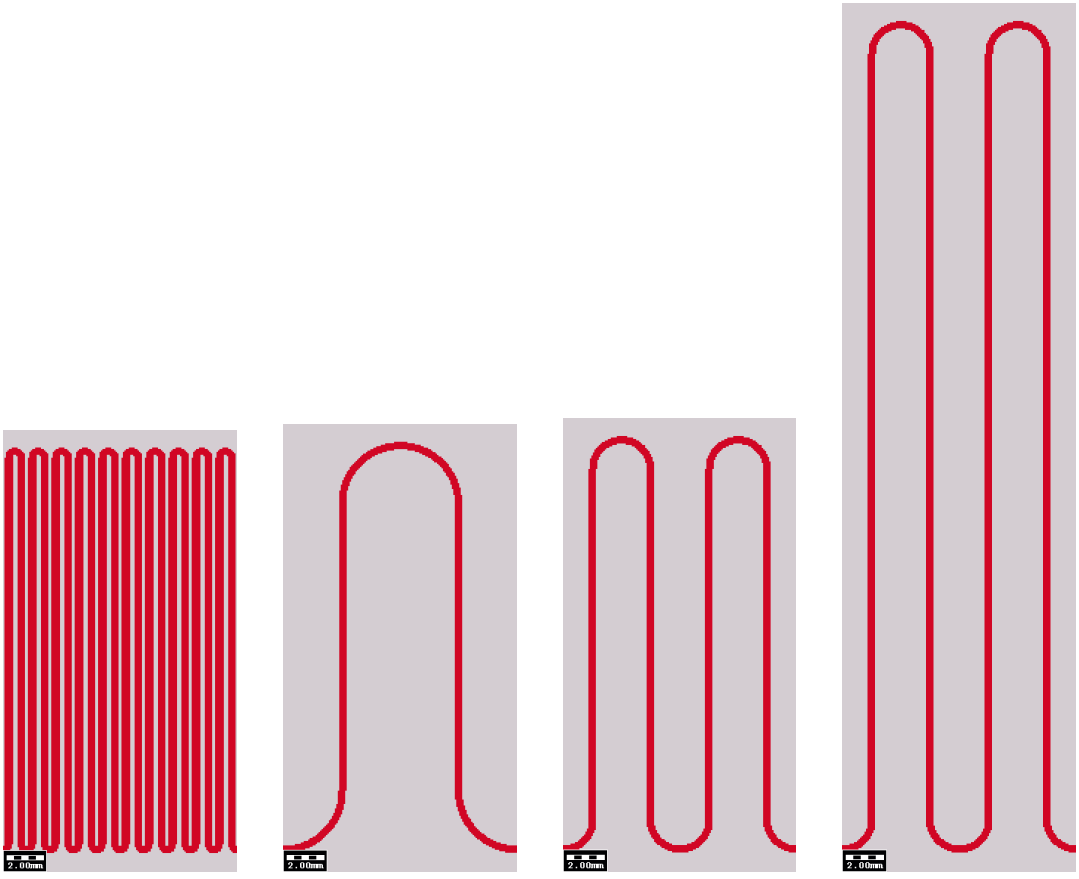

a) b) c) d)

FIGURE 4. *Illustration of pleat count and pleat height. a) Height 0.875 inch (22 mm), pleat count 20/in. b) Height 0.875 inch (22 mm), pleat count 2/in. c) Height 0.875 inch (22 mm), pleat count 4/in. d) Height 1.75 inch (44 mm), pleat count 4/in.*

(Variable 3 and Variable 4 or % 3 and % 4 in the .gvm file). More details regarding the second block in the .gvm file follow in the next section.

Figure 4 and Figure 5 illustrate a few of the possibilities of the structure generation. For the two-dimensional case in Figure 4, the pleat count and pleat height are varied, as needed to reproduce [1]. The media thickness in this example is 38 micron and the grid resolution 8 micron. This resolution means that

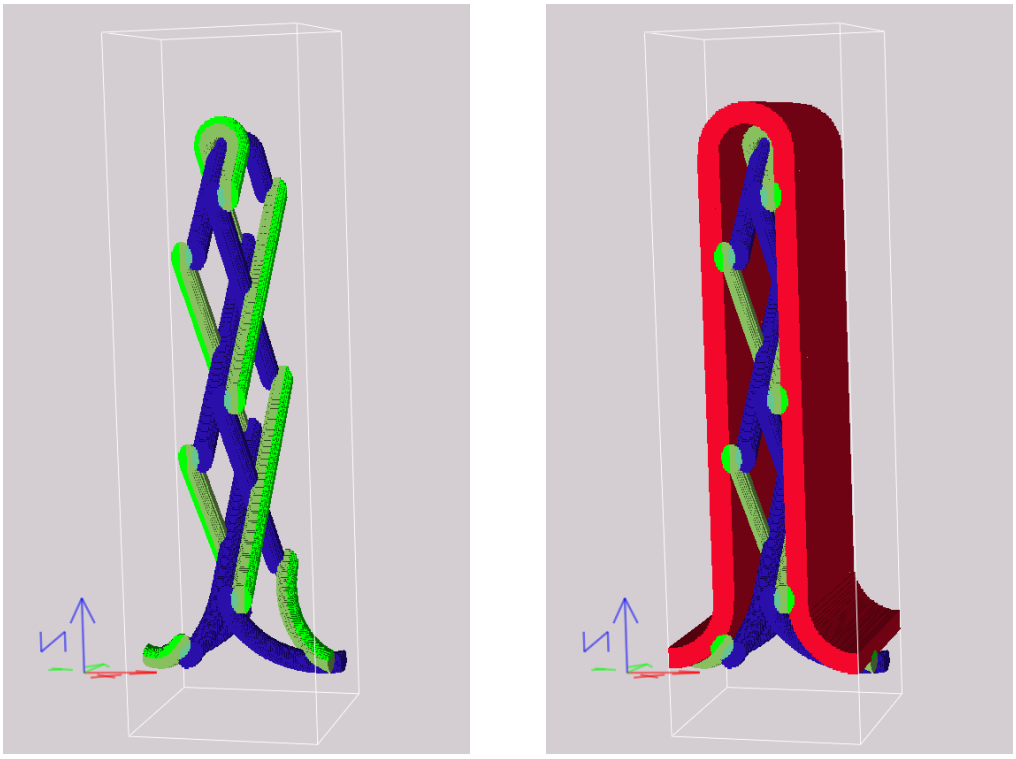

a) b)

FIGURE 5. *Three-dimensional example of a pleat with a supporting netting. a) Only support netting. Inner and outer wire shown in blue and green, respectively. b) Netting and media. The resolution, or voxel size, should be chosen so that the thickness of the media (shown in red) is at least 5 cells.*

effectively a 40 micron media will be computed. Note that using a smaller resolution such as 2 micron (which is needed to properly resolve 38 micron) would result in a 16 times (4 times 4) bigger computational problem. In 3 dimensions, this effect of grid refinement is even worse: a 4 times smaller mesh size results in a 64 times bigger computational setup. It is one of the points of this study to show that such precision is not necessary in some cases. Industrially relevant results such as the pressure drop automation by simulation can be achieved in acceptable simulation times, such as 24 hours in this case. The higher resolution computations are of course also automatically doable, but should be restricted to particularly interesting cases, and not be used for a 3-dimensional parameter study.

Such individual cases are considered in the case of the supporting structures. Here, a 3-dimensional computational domain must be considered because the support structures add a variation in the depth-direction of the pleat. Figure 5 a) shows only the support structure. For this netting, the inner and outer wires are shown for better comprehension in green and blue, with slight color differences where they overlap. For the flow, these solid wires are obstacles. In Figure 5 b), in addition to the netting also the filter media is shown. The red cells are porous, or permeable cells, i.e. the gas or liquid flows through these cells. In the case of a single layered media, the permeability of the red cells is set to that of the filter media. For layered materials, the permeability of each individual layer must be known and specified.

3. Computation of the Pressure Drop

3.1. **Notation.** Without loss of generality, the repetitive unit is a rectangular domain $\Omega = [0, l_x] \times [0, l_y] \times [0, l_z]$. The width of the pleat l_x corresponds directly to the pleat count. For example, if the pleat count is n pleats per inch, then the width is $25.4/n\,mm$, since $1\,in = 25.4\,mm$ holds. The height of the pleat together with the length of the inflow and outflow regions is denoted by l_z. The depth of the pleat is denoted by l_y. For two-dimensional computations, $l_y = 0$. Because we use a uniform Cartesian grid, we assume that

$l_x = n_x h, l_y = n_y h$ and $l_z = n_z h$, i.e. that the computational domain Ω is made up of $n_x \times n_y \times n_z$ cubic cells of volume h^3.

The volume occupied by the solid cells that result from a support structure is denoted by G. For example, the green and blue cells in Figure 5 are solid cells.

In the depth and width direction, periodic boundary conditions for the velocity and pressure are used because we compute exactly on a repetitive unit. This gives a computational domain that is twice the size in a direction than the more usual symmetry boundary conditions as used for example in [1]. In the height direction, we also use periodic boundary conditions for pressure and velocity. This is not very common but has been done successfully by our group for many years. Some discussion comparing periodic boundary conditions with pressure inlet and outflow conditions in the flow direction will follow in §4.

We assume an incompressible, creeping and stationary flow of a Newtonian liquid such as air or oil. In the Eulerian formulation as stationary Stokes-Brinkmann equations, four variable fields and one constant field describe the flow. The variable fields are the velocity and pressure, the constant field is the permeability. The velocity field $\mathbf{u} = (u, v, w)$ consists of three components indicating the contributions in the x, y and z direction, respectively. The pressure field is denoted by p.

The last field K is the permeability. We assume that all layers of the media are isotropic and extend the permeability also into the free flow regime by infinity for ease of exposition below. Following Iliev and Laptev [5], for this choice K^{-1} becomes 0 in the free flow which reduces the Stokes-Brinkmann to the Stokes equations.

$$K = \begin{cases} \begin{bmatrix} \infty & 0 & 0 \\ 0 & \infty & 0 \\ 0 & 0 & \infty \end{bmatrix} & \text{in empty cells} \\ \begin{bmatrix} \kappa_c & 0 & 0 \\ 0 & \kappa_c & 0 \\ 0 & 0 & \kappa_c \end{bmatrix} & \text{in cells of color } c, \end{cases}$$

This permeability tensor formulation is capable of handling anisotropic media in the future. The tensor would be diagonal in the directions of the media and undergo a coordinate transformation depending on the position of the media in the pleat. For example, the red cells in Figure 5 b) are permeable cells.

3.2. **Equations.** The pressure drop for a given mass flux or equivalently, given average velocity, is computed indirectly. The equations describe a setup with a defined pressure drop and the solution is then linearly scaled to reflect the desired mean velocity.

Given the pressure drop ΔP in the height direction of the pleat, we recall that the pleat height is denoted by l_z. That means that the average slope of the pressure d is given by

$$d = \frac{\Delta P}{l_z}.$$

Thus, if the true pressure is denote by P the computational pressure $p = P - dz$ is a perturbation around a constant. So even though $\mathbf{u}$ and p are periodic, P has the pressure drop ΔP. For a given pressure drop, the velocity $\mathbf{u}$ and the pressure p are then governed by the stationary Stokes-Brinkmann equations with periodic boundary conditions. Recall that under the assumption of stationarity, all time-derivatives vanish.

$$\begin{aligned} -\mu\Delta\mathbf{u} + \nabla(p + dz) + K^{-1}\mathbf{u} &= 0 \text{ in } \Omega \setminus G, && (1) \\ \nabla \cdot \mathbf{u} &= 0 \text{ in } \Omega \setminus G, && (2) \\ \mathbf{u}(x + il_x, y + jl_y, z + kl_z) &= \mathbf{u}(x, y, z) \text{ for } i, j, k \in \mathbf{Z} && (3) \\ p(x + il_x, y + jl_y, z + kl_z) &= p(x, y, z) \text{ for } i, j, k \in \mathbf{Z} \\ \mathbf{u} &= 0 \text{ on } \partial G && (4) \end{aligned}$$

Experimentalists usually prescribe the mean velocity or mass flux instead of the pressure drop. This setup is handled easily by using the linearity of the Stokes-Brinkmann equations. Once the velocity and pressure for a given pressure drop ΔP_1 have been found by solving the equations (1)-(4), one computes the average velocity in z-direction, $\bar{w}_1$. Then the pressure drop for the physical mean velocity $\bar{w}$ is $\Delta P = \frac{\bar{w}}{\bar{w}_1}\Delta P_1$.

3.3. **Discretization.** We consider the staggered grid or MAC-grid by Harlow and Welch [4] on a uniform Cartesian grid with mesh size h. On this grid, the velocity variables $\mathbf{u}$ and pressure variable p are thought to have meaning in geometrically different positions of the cell.

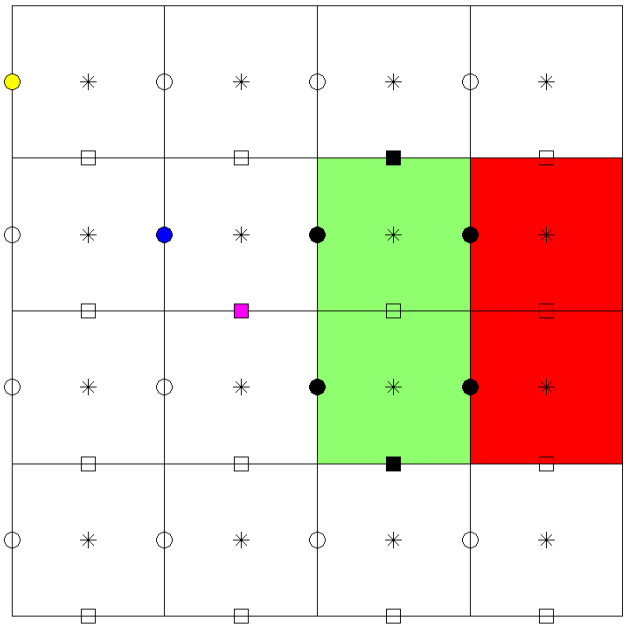

FIGURE 6. *A 4 × 4 cell domain of empty cells, solid cells (green) and permeable cells (red). On a staggered grid, the pressure variables are defined in the center of the cell (stars) and the velocities on the cell walls. The x-component of velocity u is defined on the left cell wall (circles) and the y-component of velocity v is defined on the lower cell wall (squares). No variables are defined at the top and right end of the domain by identification of the variables under periodicity of the domain. Full black symbols indicate cell walls were the no-slip boundary condition can be imposed directly by setting the variable at this location to zero. Full circles indicate zero horizontal velocity component and full squares indicate zero vertical velocity component. The three colorful symbols indicate the location where periodicity is explained (yellow), implementation of no-slip in the normal direction is explained (blue) and implementation of no-slip in the tangential direction is explained (magenta).*

3.3.1. *The staggered grid.* Cell centers are located at $\{0.5h, 1.5h, ..., (n_x-0.5)h\}\times\{0.5h, 1.5h, ..., (n_y-0.5)h\}\times\{0.5h, 1.5h, ..., (n_z-0.5)h\}$, and the variables have the following meaning: for $i = 1, 2, \ldots, n_x$, $j = 1, 2, \ldots, n_y$ and $k = 1, 2, \ldots, n_z$:

$$\begin{aligned}
P_{i,j,k} &\quad \text{is pressure at} &&((i-0.5)h, (j-0.5)h, (k-0.5)h),\\
U_{i,j,k} &\quad \text{is x-component of velocity at} &&((i-1.0)h, (j-0.5)h, (k-0.5)h),\\
V_{i,j,k} &\quad \text{is y-component of velocity at} &&((i-0.5)h, (j-1.0)h, (k-0.5)h),\\
W_{i,j,k} &\quad \text{is z-component of velocity at} &&((i-0.5)h, (j-0.5)h, (k-1.0)h).
\end{aligned}$$

Figure 6 illustrates the staggered grid and the meaning of the variables.

3.3.2. *Centered, forward and backward differences.* For the staggered grid, the discretization of the Laplace, gradient and divergence operators become particularly simply and satisfy the well known inf-sup conditions naturally. For the gradient operator, a backward difference is used, i.e. the pressure gradient reads

$$\nabla p = \big(\frac{P_i - P_{i-1}}{h}, \frac{P_j - P_{j-1}}{h}, \frac{P_k - P_{k-1}}{h}\big)^T.$$

One may think of the components as being meaningful on the respective cell wall, were the u, v and w variables live. The divergence of the velocity field is discretized by

$$\nabla \cdot \mathbf{u} = \frac{U_{i+1} - U_i + V_{j+1} - V_j + W_{k+1} - W_k}{h}.$$

One may think of each of the three differences as being meaningful in the cell center, where the p variable lives, and due to this collocation it is reasonable to add them up. Finally, with these differences, $-\Delta = -\nabla\cdot\nabla$ holds for the discrete Laplacian. More details can be found for example in [10].

Permeable cells were not used in [4], so we follow [5]: Since permeability multiplies a velocity, the two permeability values from the neighboring cells must be aggregated. We use the harmonic average

$$\kappa = \left(\frac{\kappa_1^{-1}+\kappa_2^{-1}}{2}\right)^{-1}.$$

The formula also expresses the computation of the permeability across the the interface between permeable and empty cells, if one interprets $\infty^{-1}=0$ and $0^{-1}=\infty$.

3.3.3. *The standard formulas.* We combine the equations above and for ease of notation give the details for 2 space dimensions only. The third dimension behaves just like the tangential direction in 2 space dimensions. The directions are x and z due to our convention that the pleat depth occurs in the y-direction.

For any permeable or empty cell whose 4 face neighbors are also porous or empty, the 4 equations for the 4 variables related to this cell are

$$-\mu\frac{U_{i-1,k}+U_{i,k-1}-4U_{i,k}+U_{i+1,k}+U_{i,k+1}}{h^2}+\frac{P_{i+1,k}-P_{i,k}}{h}+\left(\frac{\kappa_{i-1,k}^{-1}+\kappa_{i,k}^{-1}}{2}\right)^{-1}U_{i,k} = 0, \quad (5)$$

$$-\mu\frac{W_{i-1,k}+W_{i,k-1}-4W_{i,k}+W_{i+1,k}+W_{i,k+1}}{h^2}+\frac{P_{i,k+1}-P_{i,k}}{h}+\left(\frac{\kappa_{i,k-1}^{-1}+\kappa_{i,k}^{-1}}{2}\right)^{-1}W_{i,k} = -d, \quad (6)$$

$$\frac{U_{i+1,k}-U_{i,k}}{h}+\frac{W_{i,k+1}-W_{i,k}}{h} = 0. \quad (7)$$

Note that the given pressure drop results in the right hand side forcing term $-d$.

3.3.4. *Periodic boundary conditions.* In the staggered grid setting, a periodic boundary condition may be thought of as no boundary condition at all. Pairs of opposite sides of the domain are identified and this is reflected in the variables. We illustrate periodicity at the location with the yellow circle in Figure 6. Using that $U_{0,4}$ is identified with $U_{4,4}$, $U_{1,5}$ is identified with $U_{1,1}$ and $P_{0,4}$ is identified with $P_{4,4}$, we have

$$\begin{aligned}-\mu\frac{U_{0,4}+U_{1,3}-4U_{1,4}+U_{2,4}+U_{1,5}}{h^2}+\frac{P_{1,4}-P_{0,4}}{h} &= \\ -\mu\frac{U_{4,4}+U_{1,3}-4U_{1,4}+U_{2,4}+U_{1,1}}{h^2}+\frac{P_{1,4}-P_{4,4}}{h} &= 0\end{aligned}$$

3.3.5. *No-slip boundary condition in the normal direction.* The no-slip boundary condition specifies that the velocity is zero on the boundary. In the normal direction, this means that no material transport can occur from the fluid into the solid. This boundary condition occurs in the locations with solid black symbols in Figure 6. We illustrate how no-slip in the normal direction influences the formulas for the neighboring cells by considering (5) at the location that is marked by the blue circle in Figure 6. Using $U_{3,3}=0$, yields

$$\begin{aligned}-\mu\frac{U_{1,3}+U_{2,2}-4U_{2,3}+U_{3,3}+U_{2,4}}{h^2}+\frac{P_{2,3}-P_{1,3}}{h} &= \\ -\mu\frac{U_{1,3}+U_{2,2}-4U_{2,3}+U_{2,4}}{h^2}+\frac{P_{3,3}-P_{2,3}}{h} &= 0.\end{aligned}$$

Also, the divergence is influenced for the cell right of the blue circle. Using $U_{3,3}=0$, (7) becomes

$$\frac{U_{3,3}-U_{2,3}}{h}+\frac{W_{2,4}-W_{2,3}}{h}=\frac{-U_{2,3}}{h}+\frac{W_{2,4}-W_{2,3}}{h}=0$$

3.3.6. *No-slip boundary condition in the tangential direction.* In the tangential direction, the zero-velocity condition cannot be implemented by simply setting a variable to zero. Instead, a mirror condition is used, which was already mentioned in [4] and probably much older. We illustrate how no-slip in the tangential direction influences the formulas for the neighboring cells by considering (6) at the location that is marked by the magenta square in Figure 6. Using $W_{3,3}=-W_{2,3}$, we obtain

$$\begin{aligned}-\mu\frac{W_{1,3}+W_{2,2}-4W_{2,3}+W_{3,3}+W_{2,4}}{h^2}+\frac{P_{2,3}-P_{2,2}}{h} &= \\ -\mu\frac{W_{1,3}+W_{2,2}-5W_{2,3}+W_{2,4}}{h^2}+\frac{P_{3,3}-P_{2,3}}{h} &= -d.\end{aligned}$$

3.4. **Solution.** Following Cheng and Wiegmann [2], the Semi-Implicit Method for Pressure-Linked Equation (SIMPLE) Algorithm by Patankar and Spalding [6] is adopted. SIMPLE is essentially a guess-and-correct procedure for the calculation of pressure and velocities on the staggered grid shown in Figure 6. An initial pressure field P^* is guessed to initialize the calculation. The velocities are then solved from the discretised momentum equations (5) and (6).

$$\begin{aligned} a^U_{i,k}U^*_{i,k} &= \Sigma a^u_{nb}U^*_{nb} + (P^*_{i-1,k} - P^*_{i,k})A^U_{i,k} + b^U_{i,k} && (8)\\ a^W_{i,k}W^*_{i,k} &= \Sigma a^v_{nb}W^*_{nb} + (P^*_{i,k-1} - P^*_{i,k})A^W_{i,k} + b^W_{i,k}, && (9)\end{aligned}$$

Here the notation nb means "neighbor" cells. If we define the pressure and velocities decomposed into a guessed and corrected value,

$$\begin{aligned} P &= P^* + P'\\ U &= U^* + U'\\ V &= W^* + W', \end{aligned}$$

we obtain, by subtracting the equations (8) and (9) from the re-written equations (5) and (6):

$$\begin{aligned} a^U_{i,k}U'_{i,k} &= \Sigma a^u_{nb}U'_{nb} + (P'_{i-1,k} - P'_{i,k})A^U_{i,k} && (10)\\ a^W_{i,k}W'_{i,k} &= \Sigma a^v_{nb}W'_{nb} + (P'_{i,k-1} - P'_{i,k})A^W_{i,k}. && (11)\end{aligned}$$

In the SIMPLE algorithm, $\Sigma a^u_{nb}U'_{nb}$ and $\Sigma a^v_{nb}W'_{nb}$ are dropped. This does not affect the final solution because the pressure correction and velocity corrections will all be zero in a converged solution. Therefore, we obtain

$$\begin{aligned} U'_{i,k} &= (P'_{i-1,k} - P'_{i,k})\frac{A^U_{i,k}}{a^U_{i,k}} && (12)\\ W'_{i,k} &= (P'_{i,k-1} - P'_{i,k})\frac{A^W_{i,k}}{a^W_{i,k}}. && (13)\end{aligned}$$

The correct velocities become

$$\begin{aligned} U_{i,k} &= U^*_{i,k} + (P'_{i-1,k} - P'_{i,k})\frac{A^U_{i,k}}{a^U_{i,k}} && (14)\\ W_{i,k} &= W^*_{i,k} + (P'_{i,k-1} - P'_{i,k})\frac{A^W_{i,k}}{a^W_{i,k}}, && (15)\end{aligned}$$

and similarly,

$$\begin{aligned} U_{i+1,k} &= U^*_{i+1,k} + (P'_{i,k} - P'_{i+1,k})\frac{A^U_{i+1,k}}{a^U_{i+1,k}} && (16)\\ W_{i,k+1} &= W^*_{i,k+1} + (P'_{i,k} - P'_{i,k+1})\frac{A^W_{i,k+1}}{a^W_{i,k+1}}. && (17)\end{aligned}$$

Substituting equations (14) - (17) into the continuity equation (7), the pressure-correction equation is found as follows:

$$a^P_{i,k}P'_{i,k} = a^P_{i+1,k}P'_{i+1,k} + a^P_{i-1,k}P'_{i-1,k} + a^P_{i,k+1}P'_{i,k+1} + a^P_{i,k-1}P'_{i,k-1} + b^P_{i,k}, \quad (18)$$

where

$$\begin{aligned} b^P_{i,k} &= U'_{i+1,k} - U'_{i,k} + W'_{i,k+1} - W'_{i,k},\\ a^P_{i,k} &= a^P_{i+1,k} + a^P_{i-1,k} + a^P_{i,k+1} + a^P_{i,k-1}. \end{aligned}$$

Once the pressure correction is known, velocity corrections can be obtained with equations (10) and (11), and the correct pressure and velocity fields are obtained. Because of the simplification from equations (10) and (11) to (12) and (13), it is possible to obtain a large pressure correction based on a poorly guessed pressure field. Under-relaxation is hence used during the iterative process.

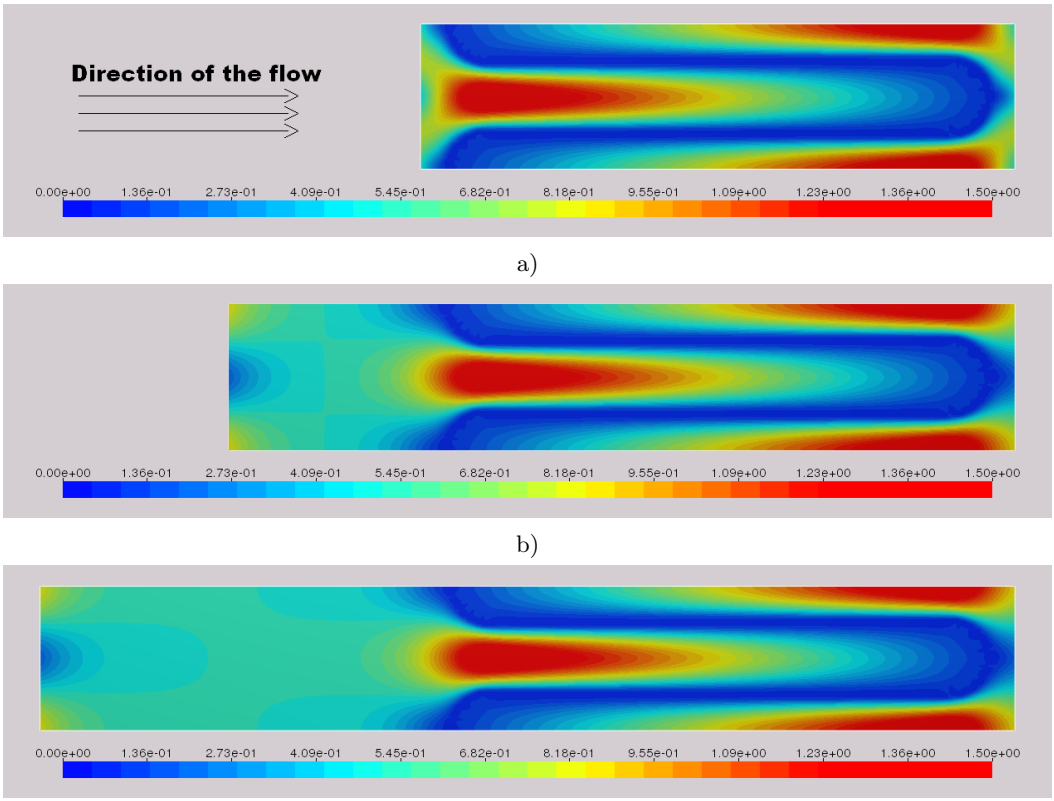

FIGURE 7. *a) Magnitude of velocity [m/s] for media 213, pleat height 0.875 in and pleat count 4. b) Same as a) with additional inlet of ca. 8 mm. c) Same as a) with additional inlet of ca. 16 mm.*

4. RESULTS

4.1. **Pleated air filter without supporting mesh.** Chen et al.[1] presented a numerial model to optimize the design of pleated filter panels. They consider air flow through 6 filter media with permeabilities listed in Table 1. For each media they consider 4 different pleat heights of 0.0875 inch, 1.75 inch, 3.5 inch and 5.25 inch and vary the pleat count for each of these 24 combinations from 2 pleats per inch to 20 pleats per inch.

Grade no.	DOP Efficiency	Permeability $\kappa[m^2]$	Thickness	Base weight $[g/m^2]$
252	99.99 % ULPA	7.25e-13	0.38	73
213	99.985% HEPA	1.03e-12	0.38	73
233	98.5 %	2.26e-12	0.38	73
220	95 %	3.20e-12	0.38	73
224	90-95 % ASHRAE	7.68e-12	0.38	73
229	80-90 % ASHRAE	1.10e-07	0.38	73

TABLE 1. Permeabilities of 6 filter media considered in [1].

Inlet length $[mm]$	$\Delta P[Pa]$
1	470.6
9	473.0
17	473.6

TABLE 2. Pressure drop for varying inlet, media 213, height 0.875 inch, velocity 100 fpm.

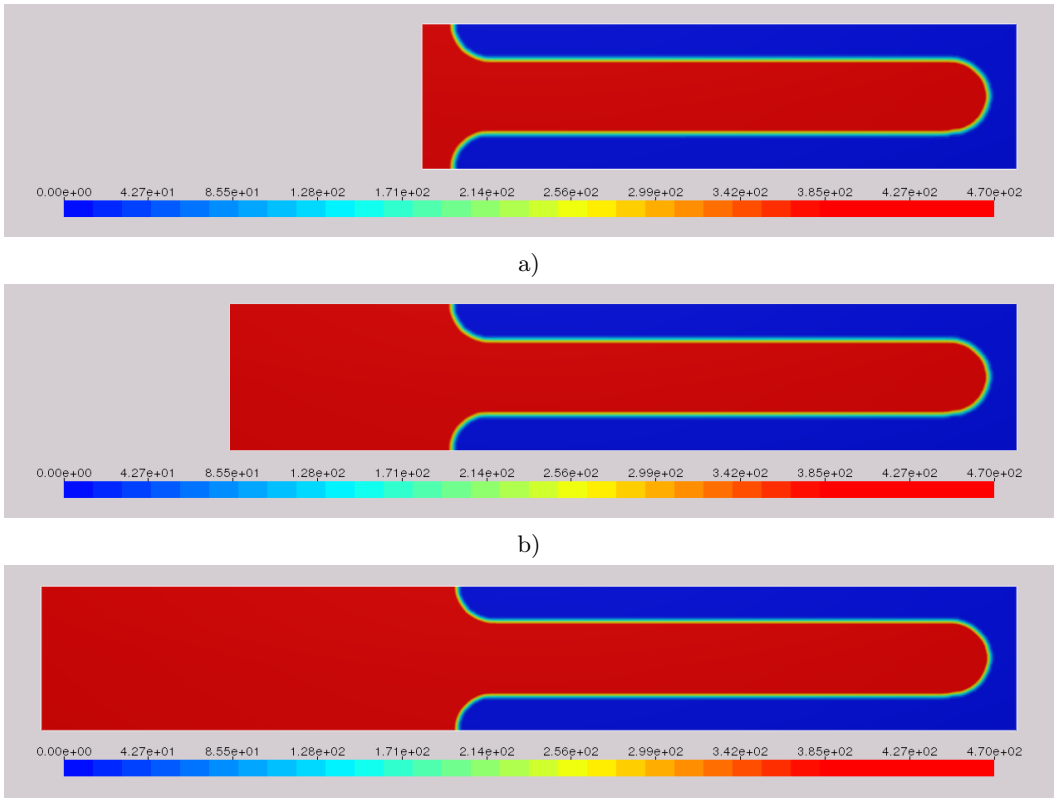

FIGURE 8. *a) Pressure [Pa] for media 213, pleat height 0.875 in and pleat count 4. b) Same as a) with additional inlet of ca. 8 mm. c) Same as a) with additional inlet of ca. 16 mm.*

Figure 4 gives an illustration about the difference in pleat count from 20 to 2 and the variation in height. The highest pleat under consideration is three times as high as the one shown in Figure 4d).

We reproduce the results from [1] in spite of several technical differences. Their finite element approach is replaced by a finite volume approach. We use periodic boundary conditions and much shorter inlets and outlets. Periodicity in the lateral direction leads to computations on a complete pleat rather than a symmetry cell as in [1] which is half a pleat. More importantly, periodic boundary conditions in the flow direction are used, which do not explicitly impose a constant velocity on any line perpendicular to the flow as it is present in [1]. This may be the reason why we may work with a much shorter inlet. Finally, here the pleat ends are rounded rather than square as in [1].

From previous experience, the resolution was chosen at 80 micron so that the thickness of the media is about 5 grid cells. This means that we effectively compute for a 40 micron media and not a 38 micron media, because the long vertical parts of the media are 5 cells wide.

In order to minimize the computation time, we first studied the influence of the length of the inlet on the computed pressure drop. Figure 7 a) — c) show the magnitude of the velocity for inlets of 1, 9 and 17 mm, respectively. For the shortest inlet the flow field is strongly influenced by the periodic boundary condition in the direction of the flow. For the longer two inlets in Figure 7 b) and c) the velocity distribution within the pleat is the same.

However, the predicted pressure drop hardly varies for the three cases, see Figure 8. The precise values for the pressure drop for the 3 different inlets is given in Table 2.

We convert our results from Pascal to inch of water gauge as used in [1] via $1\,[In.W.G.] = 249.08\,[Pa]$ and perform the same study as [1]. As dynamic viscosity we use $1.84e-5\,[kg/(ms)]$, the density is $1.02\,[kg/m^3]$ and the flow velocity is $100\,[fpm] = 0.508\,[m/s]$. The striking agreement of the results is immanent from

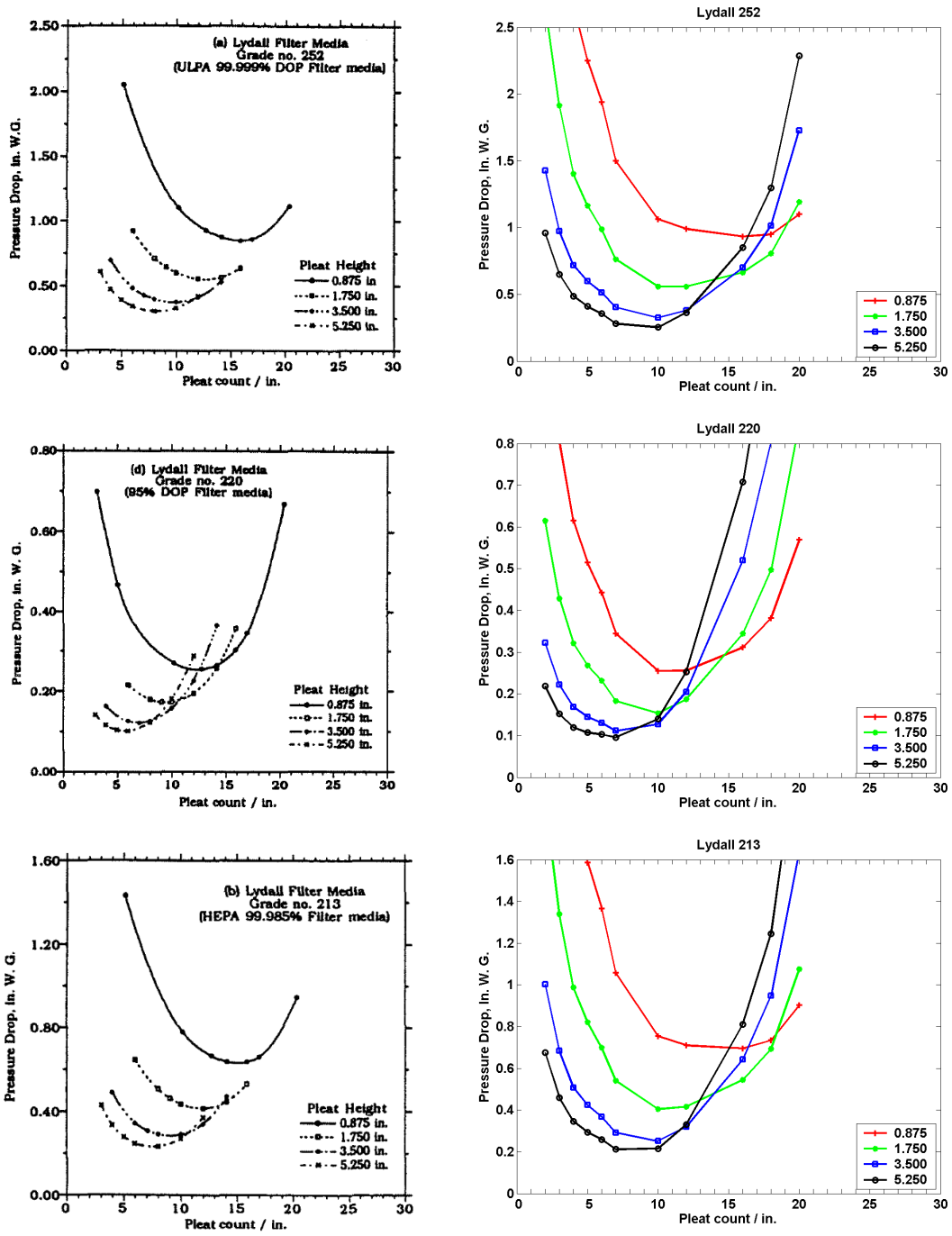

FIGURE 9. *Initial pressure drop as a function of pleat count and pleat height for 3 filter media at approaching velocity 100 fpm from* [1] *(left) and computed with GeoDict (right).*

Figure 9 and Figure 10. In particular, the same pleat parameters are found to be optimal, i.e. to have the lowest pressure drop, as in [1].

4.2. **Cartridge oil filter with a support structure in the outflow channel.** As second example, we consider cartridge oil filters. This means that in reality the pleats are not parallel as in the previous case, but

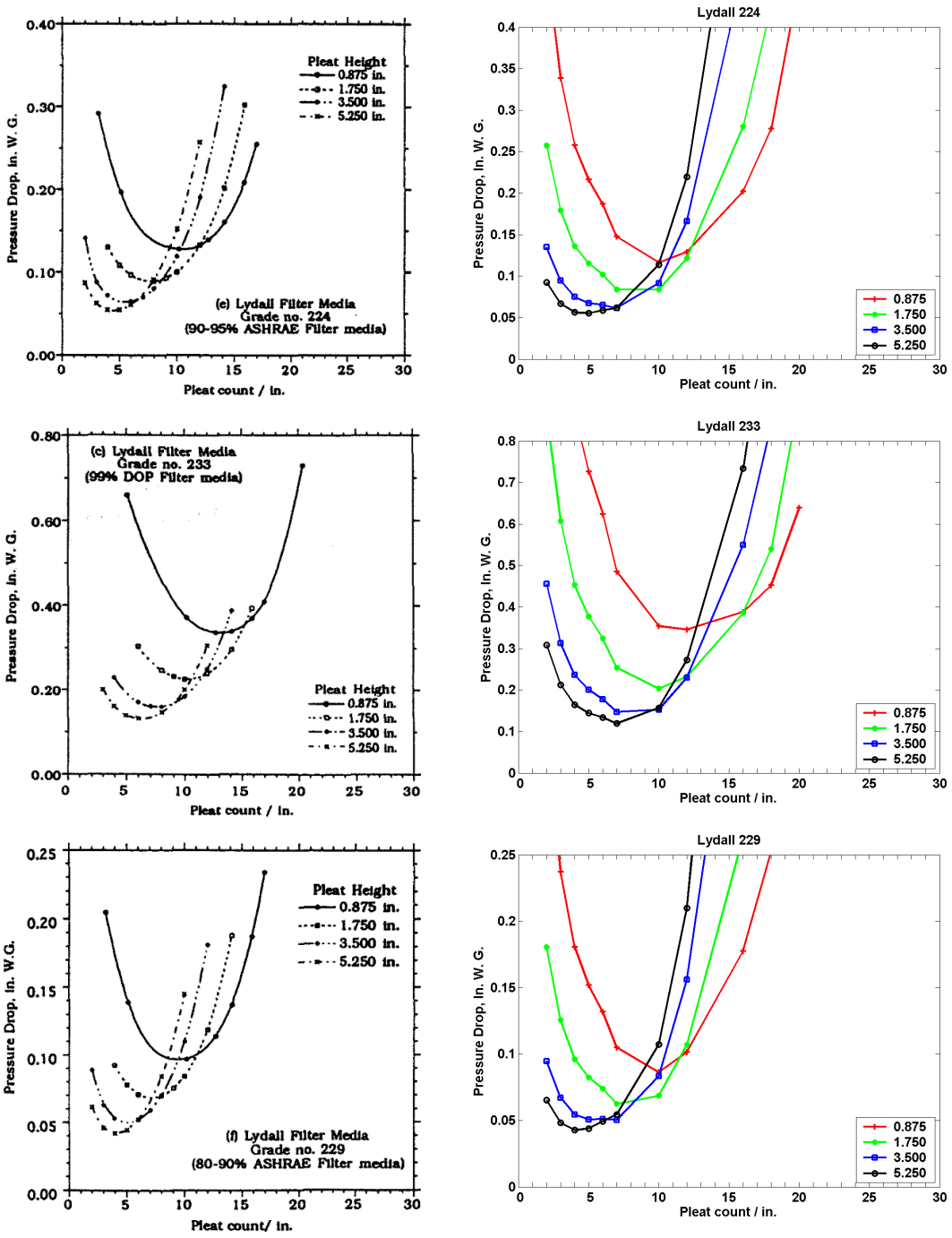

FIGURE 10. *Initial pressure drop as a function of pleat count and pleat height for 3 filter media at approaching velocity 100 fpm from* [1] *(left) and computed with GeoDict (right).*

are more open in the inflow region than in the outflow region. Another difference is that for the pressures occurring in this regime, a support structure is required that keeps the outflow channels of the pleat open. The support structure thus has a mechanical function that is not modeled, and influences the pressure by obstructing the flow in the outflow channel and effectively reducing the available surface area of the

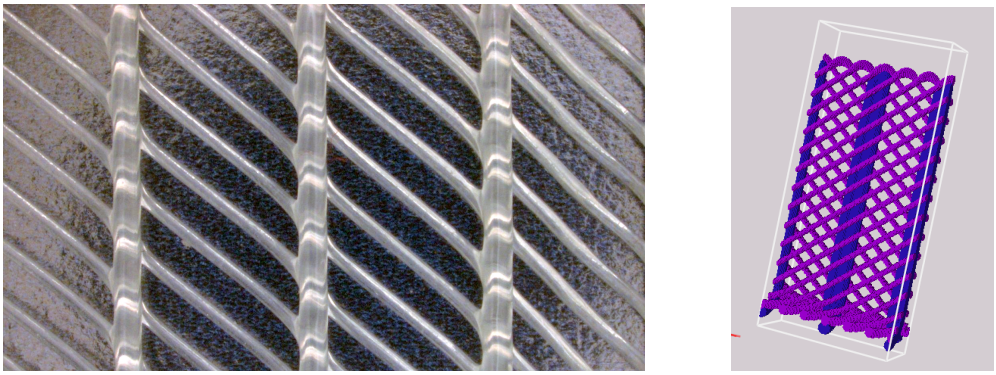

a) b)

FIGURE 11. *SEM image of a Delstar netting and computer model of a similar pleated netting.*

filter media. Different from the previous example, models including support structures must be fully three-dimensional. Figure 11 shows a scanning electron image of a standard supporting media from Delstar and a computer model of the pleated netting.

Pleat shape	$\Delta P[Pa]$
Wide outflow channel with thick wire, Figure 12 a) and Figure 13 a)	307000
Wide outflow channel with thin wire, Figure 12 b) and Figure 13 b)	275000
Narrow outflow channel, Figure 12 c) and Figure 13 c)	405000

TABLE 3. Pressure drop depending on the width of the outflow channel and the wire thickness.

Computations of oil flow through such structures have been done by our group for many years. Unfortunately, we were not permitted to show the agreement of experimental data with our simulations both for the SuFiS solver [5] and the Parpac solver [11]. However, we can compare results from the new Explicit Finite Volume Stokes solver (EFV) [2] with those for the well-established SuFiS solver [5]. Due to symmetry conditions in the depth direction, SuFiS generally computes a pressure drop that is about 2-3% higher than the new solver. Symmetry boundary conditions can be imposed in EFV by computing the pressure drop on a domain that is twice the size of the original one, which is created by reflecting the pleat in the depth direction. For symmetry boundary conditions, the results for SuFiS and EFV differ only by about 0.5%.

We consider three pleats. Two have the same outflow channel width of $720\,[\mu m]$ and one has an outflow channel of width $400\,[\mu m]$. Between the first two pleats, the thickness of the ellipsoid-shaped wires is varied. The mean flow velocity is $0.150\,[m/s]$, the oil density is $850\,[kg/m^3]$ and the oil viscosity is $0.172\,[kg/(ms)]$.

In Figure 12 and Figure 13, the flow direction is from right to left. In Figure 12, the magnitude of the flow velocity is depicted. The highest velocity occurs near the end of the outflow channel and near the end of the inflow channel. This is due to the fact that much oil is transported through these areas that diffuses from the inflow channel to the outflow channel along the length of the pleat. A good design of the support structure should lead to almost the same pressure drop as if this structure is not present. For the thicker wires in Figure 12 a) and the narrow channel in Figure 12 c), this criteria is violated: higher velocities at the end of the outflow channel than at the beginning of the inflow channel indicate an imbalance in the design.

In Figure 13, the distribution of the pressure is depicted. It illustrates why the pressure drop is 10% higher for the wide channel with thick wires and more than 30% higher than for the wide channel with thin wires. In both, Figure 13 a) and even more so in Figure 13 c), there is a significant variation in the pressure in the outflow channel. In the design in Figure 13 b), the pressure is close to constant in the outflow channel. Thus, in Figure 13 a) and c) there is an additional pressure drop due to the channel and support structure design on top of the pressure drop due to the filter media.

The lowest pressure drop occurs without support structure. But in this case the pleat would collapse and the outflow channel width would be zero. To successfully perform pleat design by computer simulations, the operator must also consider the elastic deformation of the filter media in interaction with the support structure. This is the subject of further study.

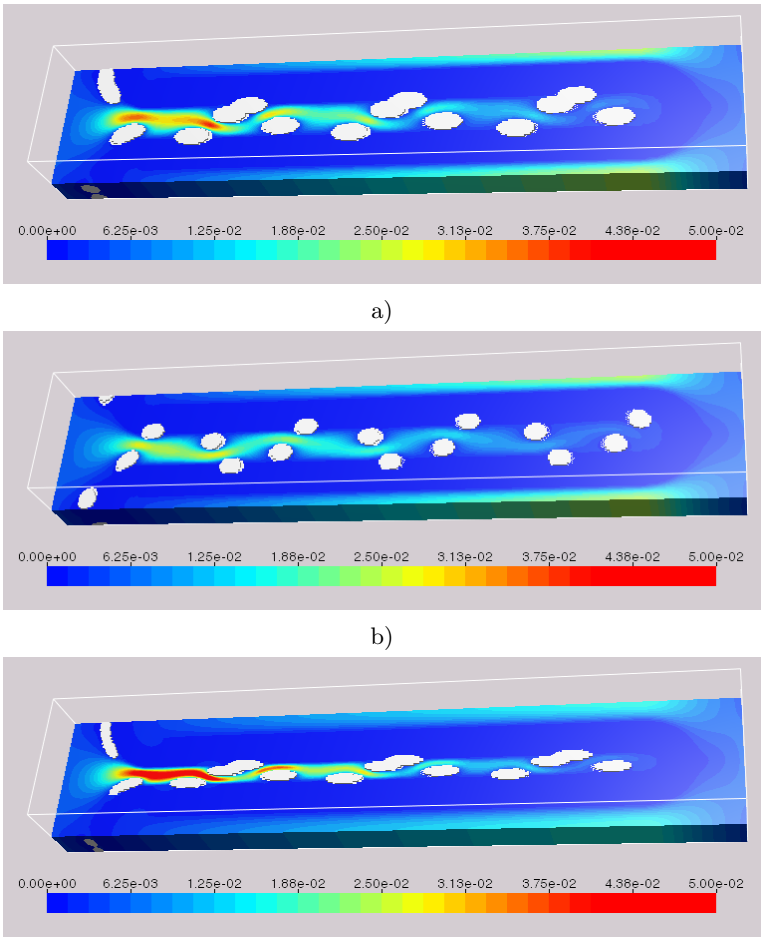

FIGURE 12. *a) Velocity for* $720\,[\mu m]$ *channel with wide wires. b) Velocity for* $720\,[\mu m]$ *channel with narrow wires. c) Velocity for* $400\,[\mu m]$ *channel. The highest velocities occur near the end of the outflow channel, where all the oil that has flown from the inflow channel into the outflow channel along the pleat length must pass through. Flow is from right to left.*

5. Conclusions

Pressure drop computations for optimizing simple pleated filter designs from [1] can be reproduced rapidly and automatically by two-dimensional simulations on a uniform Cartesian staggered grid using the SIMPLE method for the Stokes-Brinkmann formulation in the PleatDict module of the GeoDict software. The complete study of 6 x 4 x 14 simulations takes about 24 hours of computer time on a 3.1 GHz dual quad core desktop PC. This speed is possible because the coarsest conceivable grid was used, where the media is resolved by 5 porous cells. Due to the laminar flow regime and periodic boundary conditions, the inlet and outlet regions can be much shorter than used in [1]. The precise pleat shape can be neglected in this regime of long pleats.

The same technology can be used for three-dimensional computations for cartridge oil filters to analyze the influence of the support structure, pleat count, pleat height etc. on the pressure drop. Significant differences can be found for different designs and explained by the details of the velocity and pressure distribution in the pleat. Further work is needed to automatically incorporate the deformation of the filter media under the influence of the oil pressure and support structure.

References

[1] D. Chen, D. Y. H. Pui, and B. Y. H. Liu. Optimization of Pleated Filter Designs Using a Finite-Element Numerical Model. *Aerosol Science and Technology*, 23(4):579—590, 1995.

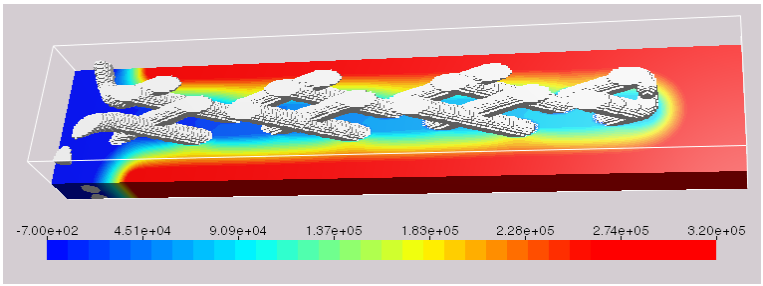

a)

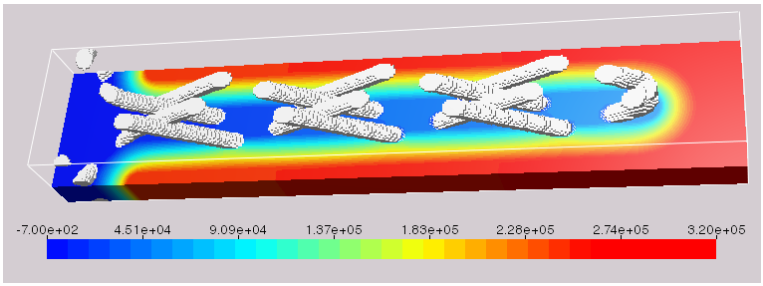

b)

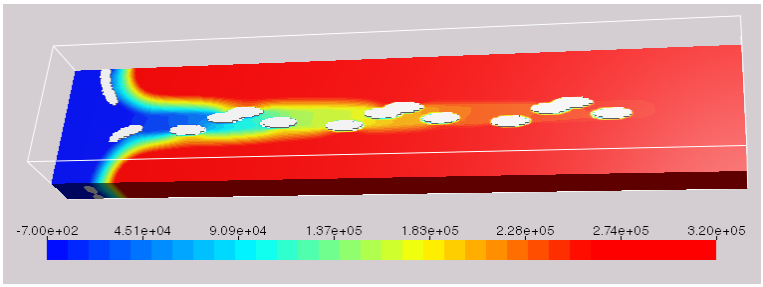

c)

FIGURE 13. *a) Pressure for* $720\,[\mu m]$ *channel with wide wires. b) Pressure for* $720\,[\mu m]$ *channel with narrow wires. c) Pressure for* $400\,[\mu m]$ *channel. The color scheme is the same for all three structures. Note the significant pressure change along the narrow outflow channel in c). Flow is from right to left.*

[2] L. Cheng and A. Wiegmann. Coupled free flow and porous media flow by EFV-Stokes. In preparation, 2009.
[3] E. Glatt, S. Rief, A. Wiegmann, M. Knefel, and E. Wegenke. Struktur und Druckverlust realer und virtueller Drahtgewebe. Submitted to Filtrieren und Separieren, 2009.
[4] F. H. Harlow and J. E. Welch. Numerical Calculation of Time-Dependent Viscous Incompressible Flow of Fluid with Free Surface. *The Physics of Fluids*, 8(12):2182—2189, 1965.
[5] O. Iliev and V. Laptev. On Numerical Simulation of Flow through Oil Filters. *J. Computers and Visualization in Science*, (6):139—146, 2004.
[6] S. V. Patankar and D. B. Spalding. A calculation procedure for heat mass and momentum transfer in three dimensional parabolic flows. *Int. J. Heat Mass Transfer*, 15:1787—1806, 1972.
[7] W. R. Ruziwa, N. S. Hanspal, A. N. Waghode, V. Nassehi, and R. J. Wakeman. Computer Modelling of Pleated Cartridge Filters for viscous fluids. *Filtration*, 4(2):136—144, 2004.
[8] W. R. Ruziwa, N. S. Hanspal, R. J. Wakeman, and V. Nassehi. Hydrodynamic Modelling of Pleated Cartridge Filter Media. In *Filtech 2003 International Conference for Filtration and Separation Technology*, volume I, pages 361—368, October 2003.
[9] R. J. Wakeman, N. S. Hanspal, A. N. Waghode, and V. Nassehi. Analysis of Pleat Crowding and Medium Compression in Pleated Cartridge Filters. In *Filtech 2005 International Conference for Filtration and Separation Technology*, volume I, pages 116—1123, October 2005.
[10] A. Wiegmann. Computation of the permeability of porous materials from their microstructure by FFF-Stokes. Technical Report 129, Fraunhofer ITWM Kaiserslautern, 2007.
[11] A. Wiegmann, S. Rief, and D. Kehrwald. Computational Study of Pressure Drop Dependence on Pleat Shape and Filter Media. In *Filtech 2007 International Conference for Filtration and Separation Technology*, volume I, pages 79—86, October 2007.